Informative singular value decomposition and its application in fault detection of planetary gearbox

OPEN ACCESS
IOP Publishing
Measurement Science and Technology
Meas. Sci. Technol. **33** (2022) 085010 (13pp)
https://doi.org/10.1088/1361-6501/ac69b0

Informative singular value decomposition and its application in fault detection of planetary gearbox

Zhaoyang Shen[1], Zhanqun Shi[1,*], Guoji Shen[2], Dong Zhen[1], Fengshou Gu[3] and Andrew Ball[3]

[1] School of Mechanical Engineering, Hebei University of Technology, Tianjin 300401, People's Republic of China
[2] Laboratory of Science and Technology on Integrated Logistics Support, National University of Defense Technology, Changsha, Hunan 410073, People's Republic of China
[3] Centre for Efficiency and Performance Engineering, University of Huddersfield, Huddersfield HD1 3DH, United Kingdom

E-mail: z_shi@hebut.edu.cn

Received 9 December 2021, revised 3 April 2022
Accepted for publication 22 April 2022
Published 12 May 2022

Abstract

The fault features of planetary gearboxes are modulated complexly and are submerged by other signal components, for its vibration signal has the characteristics of multi-source and multi transmission path. A fault detection method of planetary gearboxes based on informative singular value decomposition and envelope spectrum analysis (ISVD-ESA) is proposed in this paper. In this method, the advantage of blind source separation of singular value decomposition (SVD) method is combined with the ability of negentropy and cyclic autocorrelation (CA) in non-Gaussian characteristics recognition. The fast SVD is firstly performed to decompose the vibration signal into a series of singular value decomposition component signals (SVCSs). Secondly, the detector of negentropy combined with CA is applied to estimate the fault informativeness of each SVCS. The SVCSs are amplified by the fault informativeness and reconstructed to the out signal of ISVD. Finally, the fault features can be extracted by the ESA from the output signal of ISVD. The performance of the proposed method is verified by simulation and experimental studies. Results show that the proposed ISVD-ESA strategy can enhance the weak features of multi-modulation and accurately extract the faults of tooth tip pitting and misalignment of sun gear of the planetary gearbox.

Keywords: planetary gearbox fault detection, informative singular value decomposition, negentropy, cyclic autocorrelation, envelope spectrum

(Some figures may appear in colour only in the online journal)

* Author to whom any correspondence should be addressed.

1. Introduction

Planetary gearboxes are widely used in industrial fields [1]. In many applications, the planetary gearbox constantly operates under severe working conditions such as non-periodic heavy load condition, intermittent running conditions and so on [2, 3]. This makes the planetary gearbox is prone to failure. Once the planetary gearbox fails, the operating efficiency and service life of the whole planetary transmission system will be reduced [4]. The earlier the fault is detected, the timelier for maintenance measurements can be taken to reduce losses [5]. Consequently, it is crucial to conduct fault detection and condition monitoring for the planetary gearbox.

The fault features of planetary gearboxes are modulated complexly and often submerged by other signal components [6, 7]. Over the past years, researchers have developed many signal decomposition techniques to extract features for fault in planetary gearboxes. The fast kurtogram (FK) [8] and the wavelet transform [9] methods are proposed to extract the dominant frequency band of modulation information [10–12]; the empirical mode decomposition [13] and variational mode decomposition [14] are used to decompose the signal into a series of interrelated intrinsic mode functions (IMFs) according to different frequency bands [15], so as to reduce the influence of noise on the dominant IMFs by randomly distributing the signal noise into each IMF [16]. However, the modulation frequency of fault features in planetary gearboxes are generally in the lower frequency band, and the energy of fault feature frequency is weak and seriously affected by noise and interferences [17]. Therefore, the feature detection method based on extracting the dominant frequency band may not extract the fault features or the extracted fault features are very weak.

Recently, the singular value decomposition (SVD) method has attracted more and more attention in the fault diagnosis filed for its following advantages [18, 19]:

(a) It decomposes the signal by the decomposition of the constructed covariance matrix, so the decomposed component signals are independent of each other and can be amplified independently;
(b) It is an adaptive denoising strategy and requires very few efforts for parameter selection and therefore is convenient for calculation;
(c) The decomposed component signals are sorted according to the energy, which is conducive to information recognition.

The SVD method achieves signal decomposition by decomposing matrix form of the signal [20]. The decomposed singular value component signals (SVCSs) of SVD method are independent of each other, for the eigenvectors of the matrix are independent of each other. Therefore, the variance of each SVCS can be characterized by corresponding singular value [21]. On these bases, the SVD is used to extract the principal signal components by filtering out the component signals corresponding to incidental singular values [22–24]. However, this may filter out the fault information in the weak signal components. Researchers Zhao *et al* [25–27] developed the reweighted singular value decomposition (RSVD) method to extract weak fault information by applying the autocorrelation technique to estimate the modulations of each SVCS. Nevertheless, the variance of component signals still has an impact on autocorrelation, which may affect the accuracy of fault detection.

To detect the component signals which are full of fault information, the negentropy and cyclic autocorrelation (CA) are introduced to identify fault information and enhance the correlative decomposed component signals of SVD in the informative singular value decomposition (ISVD) method. The negentropy is a measurement to compare the probability distribution difference between a signal in time domain and another Gaussian random signal in time domain with the same co-variance [28]. It is not sensitive to the signal amplitude, but sensitive to the change of amplitude [29]. The greater the difference, the greater the negentropy. The amplitude of vibration signal of the healthy rotating machinery has the property of Gaussian distribution [18, 30]. In case of modulation such as fault, interferences and noise, it will present the non-Gaussian distribution [31]. This characteristic can be conducted to extract the informative SVCSs. Many literatures have mentioned that due to the structural characteristics of planetary gearbox, its vibration signal is mutual modulated [32, 33]. As a rotating machine, the useful vibration characteristics of planetary gearboxes have periodic modulation characteristics. The CA technology can identify the phenomenon of periodic modulation in the signal. The output signal of ISVD method is composed of different SVCSs, and the modulated fault characteristics in each SVCS are correlated. To solve this issue, the envelope spectrum analysis (ESA) is applied to detect the fault features. The performance and effectiveness of the proposed method are evaluated by both the simulation signal and the experimental data of a planetary gearbox.

The remainder of this paper is organized as follows: The fundamental principles of the ISVD and the implementation process of the proposed fault detection strategy of ISVD-ESA are detailed in section 2. The effectiveness of the proposed ISVD-ESA method in feature extraction is verified in section 3. In section 4, the actual performance of the proposed ISVD-ESA method is validated, and the superior performance of it is compared to other signal processing methods by analyzing the vibration data collected from a planetary gearbox with sun gear tip pitting and sun gear misalignment, respectively. Finally, the conclusions are summarized in section 5.

2. The fault detection method of ISVD-ESA

2.1. SVD

The SVD is a modern signal decomposition technique. It has become one of the most useful tools in mathematics and related disciplines [34]. For a preprocessed zero mean discrete digital vibration signal $\boldsymbol{x} = [x_1, x_2, x_3, \cdots, x_N]$ of N points data length, the decomposition steps of SVD signal processing are conducted as follows.

2.1.1. Matrixing of vibration signal. The vibration signal needs to be transformed into matrix structure at first. In order to make the decomposed signal components inherit more information from the raw signal, the Hankel matrix structure is used. Specifically, the matrix is constructed by the phase space reconstruction of coordinate delay method so that the elements on each anti-diagonal are equal. The structure of Hankel matrix can be shown as equation (1) [35]:

$$\mathbf{H} = \begin{bmatrix} x(1) & x(2) & \cdots & x(N-k+1) \\ x(2) & x(3) & \cdots & x(N-k+2) \\ \cdots & \cdots & \cdots & \cdots \\ x(k) & x(k+1) & \cdots & x(N) \end{bmatrix} \tag{1}$$

where the count from $x(1)$ to $x(k)$ represents the resampling length of the decomposed component signals of SVD. According to the Shannon theorem, it should be greater than or twice as long as the maximum characteristic period in the raw signal.

2.1.2. SVD of matrix. According to the matrix decomposition theorem, there are:

(a) the matrix $\mathbf{H}$ has r eigenvalues and corresponding eigenvectors;
(b) the eigenvectors corresponding to different eigenvalues of the symmetric matrix are orthogonal.

A symmetric matrix of $\mathbf{H}\mathbf{H}^{\mathrm{T}}$ or $\mathbf{H}^{\mathrm{T}}\mathbf{H}$ can be obtained by multiplying $\mathbf{H}$ and its transpose $\mathbf{H}^{\mathrm{T}}$. Then the SVD of $\mathbf{H}$ can be expressed by equation (2) [36]:

$$\mathbf{H} = \mathbf{U}\sum\mathbf{V}^{\mathrm{T}} \tag{2}$$

where $\sum = \mathrm{diag}(\sigma_1, \sigma_2, \sigma_3, \cdots, \sigma_r)$ denotes the diagonal matrix of the singular values $\sigma_i (i = 1, 2, 3, \cdots, r)$ of $\mathbf{H}$, and $\sigma_1 \geqslant \sigma_2 \geqslant \sigma_3 \geqslant \cdots \geqslant \sigma_r$. The $\mathbf{U}$ and $\mathbf{V}$ are a pair of orthogonal matrices which represent the eigenvectors of $\mathbf{H}$, and are shown in equation (3):

$$\begin{cases} \mathbf{U} = [\boldsymbol{u}_1, \boldsymbol{u}_2, \boldsymbol{u}_3, \cdots, \boldsymbol{u}_r] \in \mathbf{R}^{k \times r} \\ \mathbf{V} = [\boldsymbol{v}_1, \boldsymbol{v}_2, \boldsymbol{v}_3, \cdots, \boldsymbol{v}_r]^{\mathrm{T}} \in \mathbf{R}^{r \times N-k+1} \end{cases} \tag{3}$$

where the column vectors $\boldsymbol{v}_i$ and $\boldsymbol{u}_j$ are the base vectors in row space and column space of matrix $\mathbf{H}$ respectively.

The singular values and elements of the corresponding eigenvectors of $\mathbf{U}$ and $\mathbf{V}$ can be obtained by eliminating $\mathbf{V}$ and $\mathbf{U}$ from both sides of the matrix $\mathbf{H}\mathbf{H}^{\mathrm{T}}$ and $\mathbf{H}^{\mathrm{T}}\mathbf{H}$, the specific operations are shown in equations (4) and (5):

$$\begin{aligned} \mathbf{H}\mathbf{H}^{\mathrm{T}} &= \mathbf{U}\sum\mathbf{V}^{\mathrm{T}}\left(\mathbf{U}\sum\mathbf{V}^{\mathrm{T}}\right)^{\mathrm{T}} = \mathbf{U}\sum\mathbf{V}^{\mathrm{T}}\mathbf{V}\sum{}^{\mathrm{T}}\mathbf{U}^{\mathrm{T}} \\ &= \mathbf{U}\sum\mathbf{I}\sum{}^{\mathrm{T}}\mathbf{U}^{\mathrm{T}} = \mathbf{U}\sum{}^{2}\mathbf{U}^{\mathrm{T}} \end{aligned} \tag{4}$$

$$\begin{aligned} \mathbf{H}^{\mathrm{T}}\mathbf{H} &= \left(\mathbf{U}\sum\mathbf{V}^{\mathrm{T}}\right)^{\mathrm{T}}\mathbf{U}\sum\mathbf{V}^{\mathrm{T}} = \mathbf{V}\sum{}^{\mathrm{T}}\mathbf{U}^{\mathrm{T}}\mathbf{U}\sum\mathbf{V}^{\mathrm{T}} \\ &= \mathbf{V}\sum{}^{\mathrm{T}}\mathbf{I}\sum\mathbf{V}^{\mathrm{T}} = \mathbf{V}\sum{}^{2}\mathbf{V}^{\mathrm{T}}. \end{aligned} \tag{5}$$

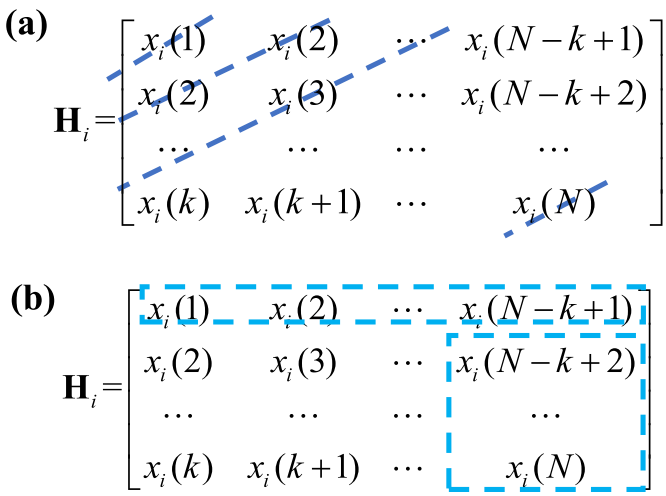

Figure 1. Transformations from Hankel matrix to component signals: (a) anti-diagonals averaging, (b) direct connection.

2.1.3. Component signals reconstruction. The matrix $\mathbf{H}$ can be decomposed into a series of different Eigen-subspaces $\mathbf{H}_i (i = 1, 2, \cdots, r)$ as presented in equation (6). However, the elements on each anti-diagonal of $\mathbf{H}_i$ are no longer equal. As shown in figure 1, two different methods can be used to transform $\mathbf{H}_i$ into component signals. In figure 1(a), each bit of the component signal is obtained by averaging the elements of $\mathbf{H}_i$ in anti-diagonals. This method can reduce random noise, but it requires a lot of computing time and storage space. Figure 1(b) provides a convenient way of obtaining component signals by splicing the first row and the last column of $\mathbf{H}_i$ directly. Reference [19] studied both the signal reconstruction methods, and pointed that the later method can save a lot of memory and computing time, but it weakens the ability to resist random errors. Therefore, the subsequent processing of the later method still need to suppress random noise

$$\begin{aligned} \mathbf{H} &= \boldsymbol{u}_1\sigma_1\boldsymbol{v}_1^{\mathrm{T}} + \boldsymbol{u}_2\sigma_2\boldsymbol{v}_2^{\mathrm{T}} + \cdots + \boldsymbol{u}_r\sigma_r\boldsymbol{v}_r^{\mathrm{T}} \\ &= \mathbf{H}_1 + \mathbf{H}_2 + \cdots + \mathbf{H}_r. \end{aligned} \tag{6}$$

2.2. Negentropy

In order to measure the informativeness of a system, Shannon proposed the concept of information entropy, which can represent the overall system state or the possibility of a certain system state occurrence. The definition of entropy for a discrete time series $\boldsymbol{x} = [x(1), x(2), x(3), \cdots, x(n)]^{\mathrm{T}}$ can be expressed with equation (7), which indicates that the entropy is closely related to the probability distribution of signal amplitude, and weakens the influence of high-energy random impulses [37]

$$H[I(x_i)] = -\sum_{i=1}^{n} p(x_i)\log p(x_i) \tag{7}$$

where $H[I(\cdot)]$ represents the information entropy, and $p(x_i)$ is the probability of the amplitude x_i to the overall signal.

It is found that the vibration signal of normal rotating machinery presents Gaussian distribution, while the fault will make the distribution change dynamically, and shows non-Gaussian characteristics. For random signals with the same mean and variance, the entropy values of Gaussian signals are the largest ones, which has been demonstrated in the central limit theorem in statistical theory. Negentropy performs well in distinguishing the Gaussian distribution and the non-Gaussian distribution of a system, and can be defined by equation (8) [38]

$$\begin{aligned} J(x) &= D[p(x)||p(x_{\text{Gauss}})] \\ &= \sum p(x)\log\frac{p(x)}{p(x_{\text{Gauss}})} \end{aligned} \tag{8}$$

where $J(x)$ represents negentropy of the signal x, $D(\cdot||\cdot)$ denotes the divergence function, which is used to measure the probability distribution difference between two signals. x_{Gauss} is a simulated Gaussian signal with the same mean and variance as the signal x. A larger value of $J(x)$ means more modulation information in the measured signal x. Since the calculation of $J(x)$ in equation (8) is very complex, an approximate function based on maximum entropy is usually used, which is shown as equation (9) [39]

$$\begin{aligned} J(x) \approx\ & k_1 E^2[G_1(x)] \\ & + k_2\{E[G_2(x)] - E[G_2(x_{\text{Gauss}})]\}^2 \end{aligned} \tag{9}$$

where k_1 and k_2 are the positive constants, $E(\cdot)$ is expectation operator, $G_1(\cdot)$ and $G_2(\cdot)$ denote non quadratic functions. For convenient calculation and obtaining stable result, $G_1(x) = \log[\cosh(x)]$ is used to detect sub Gaussian distribution, and $G_2(x) = -\mathrm{e}^{-\frac{x^2}{2}}$ is to detect super Gaussian distribution.

2.3. CA

The vibration signal of healthy rotating machinery has the property of Gaussian distribution, while that of the faulty rotating machinery has the non-Gaussian characteristic of periodic modulation. The CA is a useful tool to identify periodic modulation characteristics of signals [40, 41]. Let the sequence $x[t]$ be a cyclo-stationarity digital signal, and its autocorrelation function can be described as equation (10)

$$R_x(t,\tau) = \lim_{T\to\infty}\frac{1}{T}\sum_{t=0}^{T} x\left(t-\frac{\tau}{2}\right)x^*\left(t+\frac{\tau}{2}\right) \tag{10}$$

where $R_x(\cdot)$ represents the autocorrelation function, t is the independent variable over time, τ is the delaying time, '$*$' means the complex conjugate, and T represents the data sampling length.

Suppose $x[t]$ is composed of a stationary periodic modulation component $p[t]$ and noise $n[t]$. Then the autocorrelation of $x[t]$ can be expressed as equation (11)

$$\begin{aligned} R_x(t,\tau) = & \\ \lim_{T\to\infty}\frac{1}{T}\sum_{t=0}^{T}\Bigg[& p\left(t-\frac{\tau}{2}\right)p^*\left(t+\frac{\tau}{2}\right) + p\left(t-\frac{\tau}{2}\right)n^*\left(t+\frac{\tau}{2}\right) \\ & + n\left(t-\frac{\tau}{2}\right)p^*\left(t+\frac{\tau}{2}\right) + n\left(t-\frac{\tau}{2}\right)n^*\left(t+\frac{\tau}{2}\right)\Bigg] \\ = & E\left[p\left(t-\frac{\tau}{2}\right)p^*\left(t+\frac{\tau}{2}\right)\right] + E\left[p\left(t-\frac{\tau}{2}\right)n^*\left(t+\frac{\tau}{2}\right)\right] \\ & + E\left[n\left(t-\frac{\tau}{2}\right)p^*\left(t+\frac{\tau}{2}\right)\right] + E\left[n\left(t-\frac{\tau}{2}\right)n^*\left(t+\frac{\tau}{2}\right)\right] \end{aligned} \tag{11}$$

where $E[*]$ is expectation operator.

Because $p[t]$ is linearly independent of $n[t]$, their convolution is equal to zero. Therefore, the autocorrelation of $x[t]$ at $\tau = 0$ is shown in equation (12), which is equal to the total energy of the signal modulations

$$R_x(t,0) = E\left[p^2(t)\right] + E\left[n^2(t)\right]. \tag{12}$$

The periodic modulation has repeatability, and its relationship with respect to period T_0 can be shown as equation (13). The CA informativeness of repetitive modulation of the signal can be expressed as equation (14)

$$E\left[p^2(t)\right] = E\left[p^2(t+nT_0)\right] \tag{13}$$

$$\mathrm{CA_R} = \frac{E\left[p^2(t+nT_0)\right]}{R_x(t,0) - E\left[p^2(t)\right]} \tag{14}$$

where n is a positive integer.

2.4. The fault feature extraction method of ISVD-ESA

To detect fault features from the complex and multi-source vibration signal of planetary gearbox, an ISVD-ESA method is developed to enhance the fault source component signals and extract the fault features. The main implementation steps of the ISVD-ESA method are as follows, and its flowchart is displayed in figure 2.

Step 1: The SVD is firstly utilized to decompose the vibration signal into a series of matrices which are mutually independent and can quickly transform to SVCSs.

Since the number of k in signal matrixing is equal to the resampling length of a rectangular window, it is set to a number slightly larger than twice the number of periodic sampling points of the rotating part with the smallest frequency conversion in this work according to the Shannon theorem. To save computation, Zhao [19] analyzed the SVCSs of first 50 items. To further reduce the calculation and make full use of the high SNR of SVCSs, only the SVCSs with singular values greater than the mean of the first 50 terms are considered in the next steps.

Step 2: Estimate the fault informativeness of each SVCS by the negentropy and the CA, respectively.

The non-Gaussian informativeness of each SVCS is estimated by the negentropy as equation (9). Meanwhile, the informativeness of periodic modulation characteristics of each SVCS

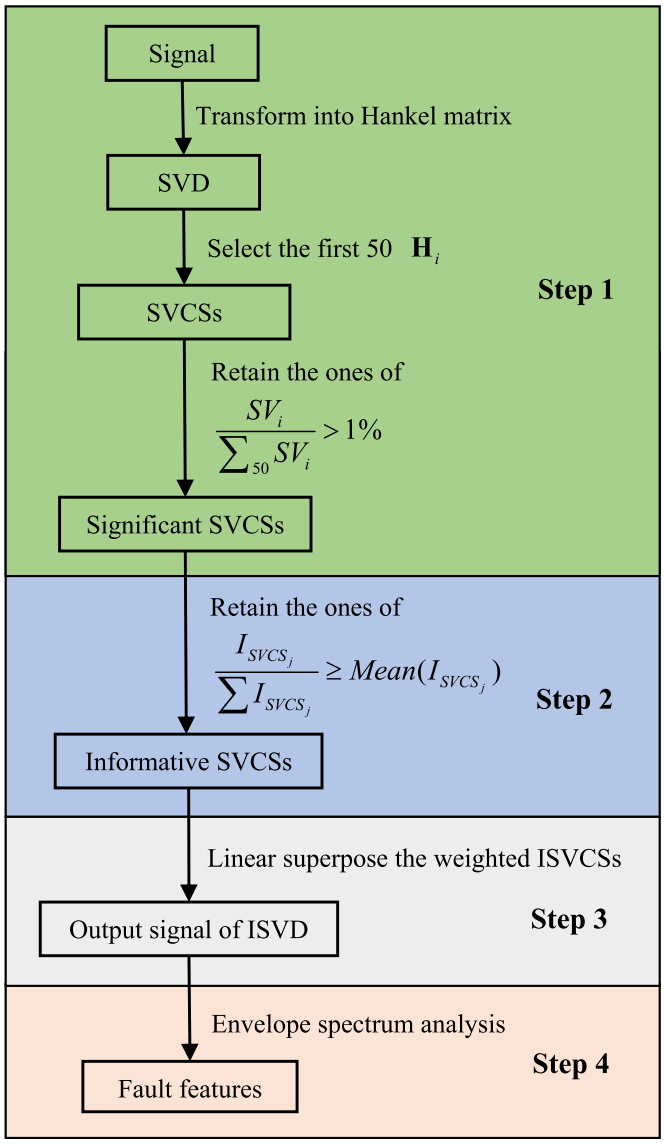

Figure 2. Flowchart of the ISVD-ESA method.

is estimated by the CA as equation (14). The weight of fault information of each SVCS is measured as equation (15). To enhance the SNR of fault information, only the SVCSs with high weight are retained

$$\mathrm{ISVCS}_j = \begin{cases} I_{\mathrm{SVCS}_j}, \dfrac{I_{\mathrm{SVCS}_j}}{\sum\limits_j I_{\mathrm{SVCS}_j}} \geqslant \mathrm{Mean}\left(I_{\mathrm{SVCS}_j}\right) \\ 0, \dfrac{I_{\mathrm{SVCS}_j}}{\sum\limits_j I_{\mathrm{SVCS}_j}} < \mathrm{Mean}\left(I_{\mathrm{SVCS}_j}\right) \end{cases}. \tag{15}$$

It should be noted that the informativeness of negentropy and CA of each SVCS is independent, and their contribution weight in signal reconstruction is equal. This means that the SVCSs with high informativeness of both characteristics will be more enhanced in the reconstructed signal.

Step 3: Calculate the contribution weight of each ISVCS in signal reconstruction and reconstruct the signal.

The contribution weight of each ISVCS is calculated by equation (16). In order to reduce the influence of signal energy on ISVCSs, each ISVCS is amplified by $1/\mathrm{SV}_j$, for the singular values corresponding to the energy of the decomposed component signals of SVD

$$\mathrm{CW}_j = \frac{\mathrm{ISVC}_j}{\sum \mathrm{ISVC}_j} \times 100\%. \tag{16}$$

Step 4: Conduct ESA of the output signal of ISVD, and identify the fault features.

3. Simulation evaluation

In this section, a numerical signal is simulated to study the performance of the proposed ISVD-ESA method in fault features extraction. The meshing frequency is the main component of the vibration signal of the general rotating machinery. Once a rotating component fails, the periodic fault frequencies of the component will be modulated to the meshing frequency. Fault characteristics of a planetary gearbox are inevitably coupled and modulated by many factors due to the complex path and attenuation in the transmission of vibration signal, and are submerged by interferences and noise. Among the local faults of the planetary gearbox, the vibration signal of sun gear fault is the most complex. In order to simulate the mentioned vibration signal properties of the planetary gearbox, the expression of local fault of sun gear signal can be described as equation (17) [42, 43]:

$$x(t) = \sum_{i=1}^{N} S_i(t) + R_i(t) \tag{17}$$

where N is the number of planetary gears. $S_i(t)$ represents the vibration response of the sun gear meshing with the ith planetary gear, $R_i(t)$ denotes the vibration response of the ith planetary gear meshing with the gear ring, and their corresponding expressions are shown in equation (18):

$$\begin{cases} S_i(t) = A_{si}(t) V_{spi}(t) \\ R_i(t) = A_{ri}(t) V_{rpi}(t) \end{cases} \tag{18}$$

where $A_{si}(t)$ and $A_{ri}(t)$ are the responses of transfer path of the ith planetary gear meshing with the sun gear and the gear ring, respectively. The transfer path responses can be simulated by the Hamming window functions, which are shown as equation (19):

$$\begin{cases} A_{si}(t) = 1 - \cos(2\pi f_c t + \frac{i}{N} 2\pi) \\ A_{ri}(t) = 1 - \cos(2\pi f_c t + \frac{i}{N} 2\pi) \end{cases} \tag{19}$$

where $V_{spi}(t)$ and $V_{rpi}(t)$ represent the modulated vibration components in the transmission process by the ith planetary gear meshing with the sun gear and the gear ring, respectively. Their corresponding expressions are shown in equation (20):

Table 1. Parameters used in the simulation signal.

Symbol	N	H	f_m	f_s	f_p	f_c	f_{sf}
Value	3	3	100	8.33	2.78	1.04	21.88
Symbol	M_1	M_2	M_3	φ	ϕ	α_1	β_1
Value	1.5	1	0.5	0	0	$\pi/3$	$\pi/3$

$$\begin{cases} V_{spi}(t) = [1+\cos(2\pi f_p t+\varphi_{pi})+\cos(2\pi f_c t+\varphi_{ci}) \\ \qquad\qquad +\cos(2\pi f_s t+\varphi_{si}) \\ \qquad\qquad +B_i(t)]\cos[2\pi f_m t+C_i(t)+\varphi_{spi}(t)] \\ V_{rpi}(t) = 1+\cos(2\pi f_p t+\phi_{pi}) \\ \qquad\qquad +\cos(2\pi f_c t+\phi_{ci})\cos[2\pi f_m t+\phi_{rpi}(t)] \end{cases} \tag{20}$$

where φ_i and ϕ_i represent the phases of ith planetary gear meshing with sun gear or gear ring, respectively. $B_i(t)$ and $C_i(t)$ respectively denote the amplitude modulation (AM) components and frequency modulation (FM) components, and their corresponding expression are formulated as equation (21):

$$\begin{cases} B_i(t) = \sum_{j=1}^{H} M_j \cos(2\pi f_{sf}+\alpha_j) \\ C_i(t) = \sum_{j=1}^{H} M'_j \cos(2\pi f_{sf}+\beta_j) \end{cases} \tag{21}$$

where H is the number of harmonic frequencies of sun gear fault, M_{ij} and M'_{ij} are amplitudes of AM and FM of the jth harmonic frequency of sun gear fault, respectively. f_{sf} denotes sun gear fault frequency. α_{ij} and β_{ij} represent the phases of jth harmonic frequency of AM and FM, respectively. The $n(t)$ indicates the white Gaussian noise to mimic the influence of operating environment.

The parameters of this vibration signal model are listed in table 1. The waveform of this simulation model is depicted in figure 3(a), and its corresponding spectrum and envelope spectrum are presented in figures 3(b) and (c), respectively. As is shown in figure 3(b), the information of the sidebands on both sides of the meshing frequency is complex. As marked by ellipses in figure 3(b), the signal is serious affected by noise. It can be seen from figure 3(c) that the interference frequencies are presented clearly, but the sun gear fault frequencies are submerged by the interferences frequency and noise.

To effectively detect the fault frequency, the proposed ISVD-ESA method is utilized to analyze the simulation signal. First, the output signal of ISVD is shown in figure 4(a), which shows stronger non-Gaussian behavior than the signal waveform in figure 3(a). The amplitude spectrum of t the output signal of ISVD is drawn in figure 4(b). It shows the modulated frequencies of $f_m-2f_{sf}, f_m-f_{sf}, f_m-f_a, f_m+f_a, f_m+f_{sf}, f_m+2f_{sf}$ and f_m+3f_{sf} are more clearer than those in figure 3(b). It is proved that ISVD method can effectively remove the noise and interferences, and retain the signal components with fault information. The envelope spectrum of ISVD-ESA is presented in figure 4(c), in which the interference except the f_c is weakened, and the fault frequency and its harmonics are enhanced and can be clearly identified. In the operation of the planetary gearbox, the vibration signal is modulated by the rotation frequency of the planetary carrier, so f_c is extracted by the ISVD-ESA. The results reveal that the ISVD-ESA method has the ability to enhance the fault features and weaken interferences.

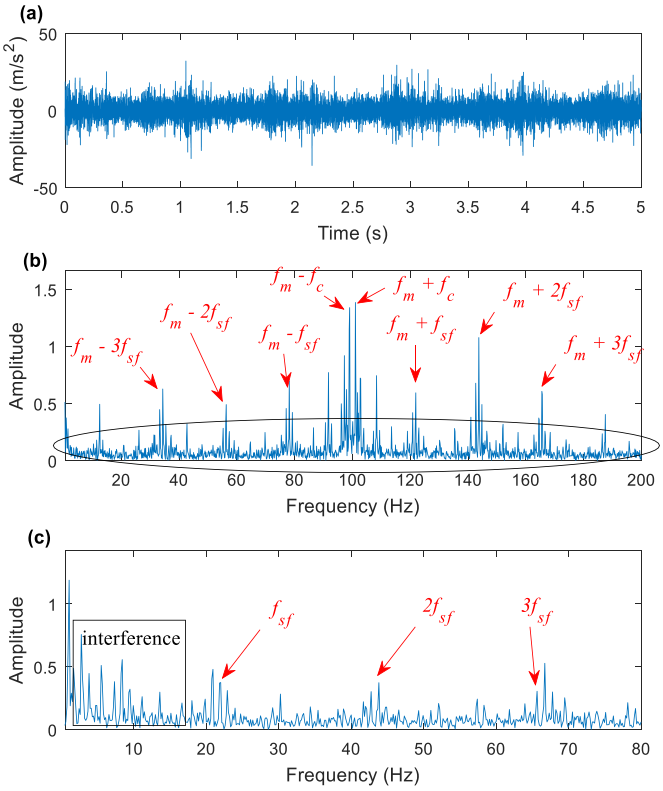

Figure 3. Simulation signal: (a) waveform, (b) the amplitude spectrum, (c) envelope spectrum.

4. Experiments validation

Since the vibration response of the sun gear fault is weak and disturbed in the collected vibration signal, the signals of sun gear fault of planetary gearbox can verify the correctness and effectiveness of the proposed ISVD-ESA method. Two general sun gear faults with tooth tip pitting and misalignment are conducted respectively on a planetary gearbox test rig. In order to present the advantages of the ISVD-ESA method, the methods of RSVD-ESA and the FK are utilized to analyze the same data for comparison.

4.1. Experimental system and data acquisition

As shown in figure 5, the experiment setup is composed of a three-phase AC motor with a rated speed of 1450 rpm, a two-stage helical gearbox, a planetary gearbox and a DC generator to provide load. The ring gear of the planetary gearbox is fixed on the platform, the sun gear is used as the input part of the power, and the planet carrier is the output part. A vibration sensor attached to the ring of planetary gearbox. The sampling frequency is 10 000 Hz, and the sampling time is 2 s. The concerned parameters of the planetary gearbox are listed in table 2.

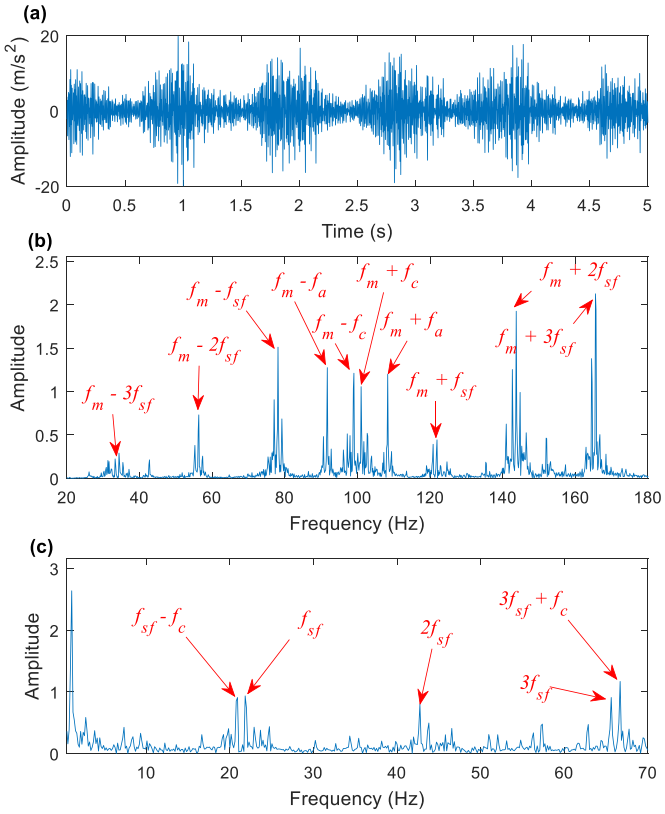

Figure 4. ISVD-ESA results: (a) waveform of ISVD processed signal, (b) amplitude spectrum, (c) envelope spectrum.

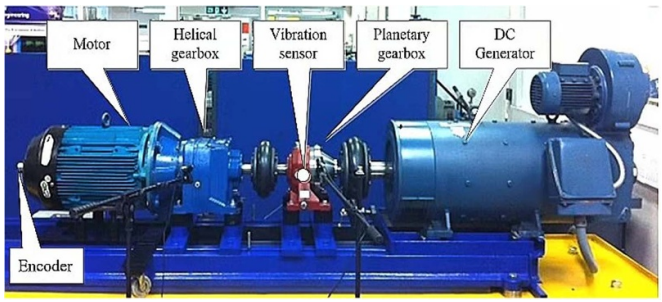

Figure 5. Experiment setup.

Table 2. Parameters of the tested planetary gearbox.

Sun gear (Z_s)	Planetary gear (Z_p)	Internal ring gear (Z_r)	Planetary gear number (N_p)	Transmission Ratio
10	26	62	3	7.2

Since the planetary gears are fixed on the planet carrier and revolve around the sun gear at the speed of the planet carrier. The relationship between each rotation frequency and meshing frequency is shown as equation (22):

$$f_m = f_c \cdot z_r = (f_{as} - f_c) \cdot z_s \tag{22}$$

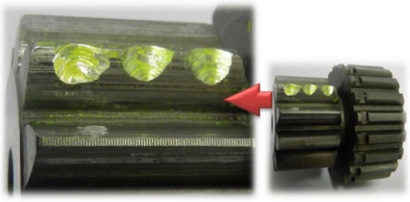

Figure 6. Tooth pitting on sun gear.

Table 3. Characteristic component frequencies of the diagnosed planetary gearbox.

Characteristic Frequency	Relationship to input frequency	Value (Hz)
Sun gear shaft (f_{as})	f_{as}	4.85
Sun gear (f_s)	$f_{as} \cdot z_r/(z_s + z_r)$	4.17
Sun gear fault (f_{sf})	$N_p \cdot f_{as} \cdot z_r/(z_s + z_r)$	12.52
Planetary gear (f_p)	$f_{as} \cdot z_s \cdot z_r/[z_p \cdot (z_s + z_r)]$	1.61
Planetary gear fault (f_{pf})	$2f_{as} \cdot z_s \cdot z_r/[z_p \cdot (z_s + z_r)]$	3.21
Planetary carrier (f_c)	$f_{as} \cdot z_s/(z_s + z_r)$	0.67
Internal ring gear fault (f_{rf})	$N_p \cdot f_{as} \cdot z_s/(z_s + z_r)$	2.02
Meshing frequency (f_m)	$f_{as} \cdot z_s \cdot z_r/(z_s + z_r)$	41.76

where f_{as} is the actual rotation frequency of the sun gear. However, the rotation frequency of the sun gear relative to the planet carrier $f_s = f_{as} - f_c$ is engaged in the meshing process.

The rotation frequency of each component can be deduced by equation (22). During one cycle of rotation of the sun gear relative to the planet carrier, each planetary gear will mesh with the fault tooth on the sun gear once. Therefore, the sun gear fault frequency is $f_{sf} = N \cdot f_s$. When a faulty planetary gear rotates for one cycle, its fault will vibrate with the sun gear and the ring gear respectively. Therefore, the planetary gear fault frequency is $f_{pf} = 2 \cdot f_m/z_p$. When the inner ring gear fails, each planetary gear vibrates with the fault within one cycle of planetary carrier rotation. Therefore, the planetary gear fault frequency is $f_{rf} = N \cdot f_c$.

4.2. Fault detection of tooth pitting of sun gear

In this case, the tooth pitting fault is exhibited in figure 6. It was created by three equidistant small artificial pits on the top of one tooth of the sun gear and along with the axial direction of tooth width. The vibration signal of the planetary gearbox under 20% rated speed and 50% rated load is collected, and the sun gear shaft speed is 291 rpm, and the characteristic frequencies are listed in table 3.

The vibration signal for the sun gear tooth pitting of the planetary gearbox is displayed in figure 7(a). It can be seen that the vibration signal is suffering from the interferences of high amplitude random pulses and random noise. The results of the amplitude spectrum and the envelope spectrum are depicted in figures 7(b) and (c), respectively. Figure 7(b) shows that the spectrum of the signal is strongly affected by noise, and the frequency of $f_m \pm f_s + 3f_c$ can be identified. However, this modulation component may be caused by the transmission process of vibration signal but no fault. The features

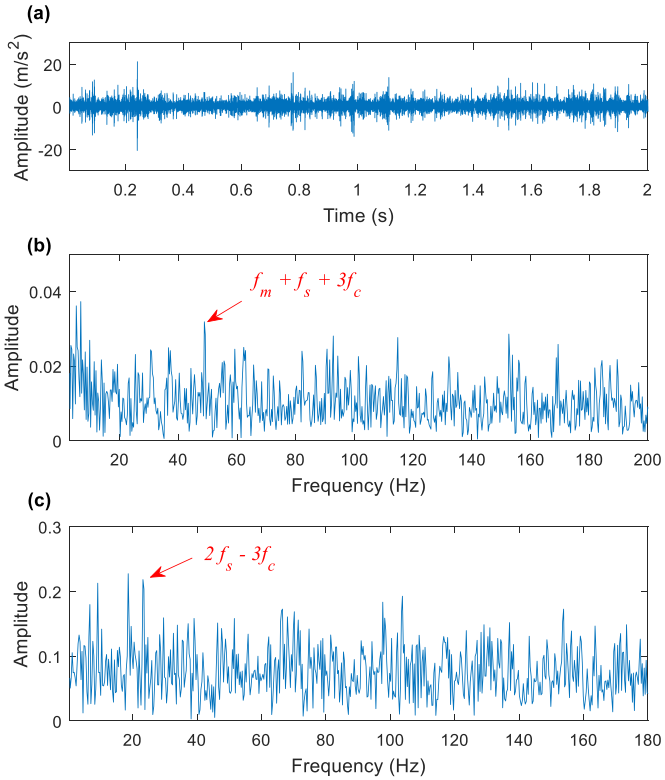

Figure 7. Experimental signal: (a) waveform, (b) the amplitude spectrum, (c) envelope spectrum.

in figure 7(c) are also seriously disturbed and submerged by noise, and the slightly prominent frequency $f_s - 3f_c$ is not a fault feature. Therefore, there is no any fault information in the amplitude spectrum and the envelope spectrum of the signal.

The proposed ISVD-ESA method is applied to extract the tooth pitting fault features of sun gear from the vibration signal. Considering the characteristic frequency of planetary gearbox, the value of parameter k of signal matrixing is set as $k = 3000$ according to step 1 of ISVD-ESA strategy. The output signal waveform of ISVD is depicted in figure 8(a). It shows that the signal has strong non-Gaussian characteristic. The ISVD-ESA result is shown in figure 8(b), from which the harmonics of second harmonic fault frequency are obviously identified. The extracted features can clearly reveal that the sun gear is faulty.

For comparison, the method of RSVD-ESA is utilized to analyze the same vibration signal which is shown in figure 7(a), the processing steps are similar with the ISVD-ESA method, and the results are drawn in figure 9. Figure 9(a) presents the time domain waveform of the output signal of RSVD. It can be seen that the periodic component in the signal is amplified and contributes greatly to the signal reconstruction. The result of RSVD-ESA is shown in figure 9(b). It shows that the meshing frequency modulated by the signal transmission characteristic frequency can be clearly identified, and the frequencies near the second harmonic frequency of sun gear fault and its sideband can be weakly identified. But these frequencies are seriously mixed by interferences and noise, and it is difficult to determine that these frequency components are related to the fault characteristics of the sun gear.

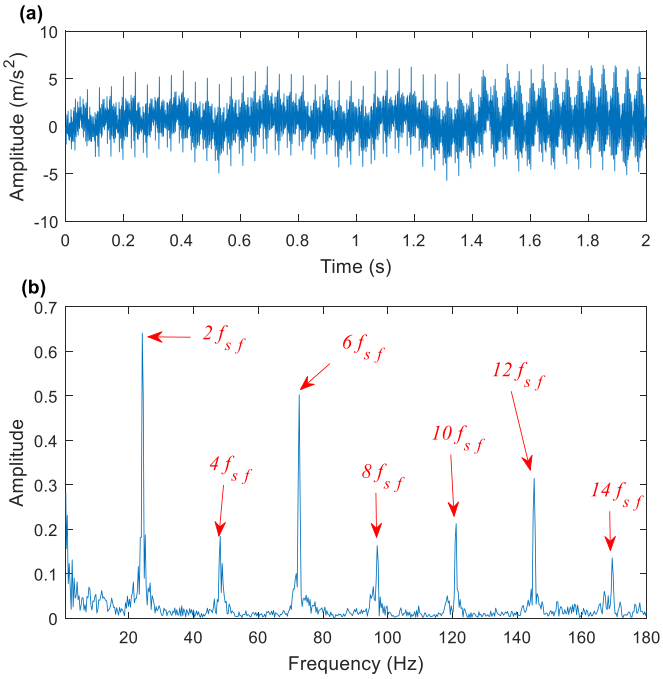

Figure 8. ISVD-ESA results: (a) waveform of ISVD processed signal, (b) envelope spectrum.

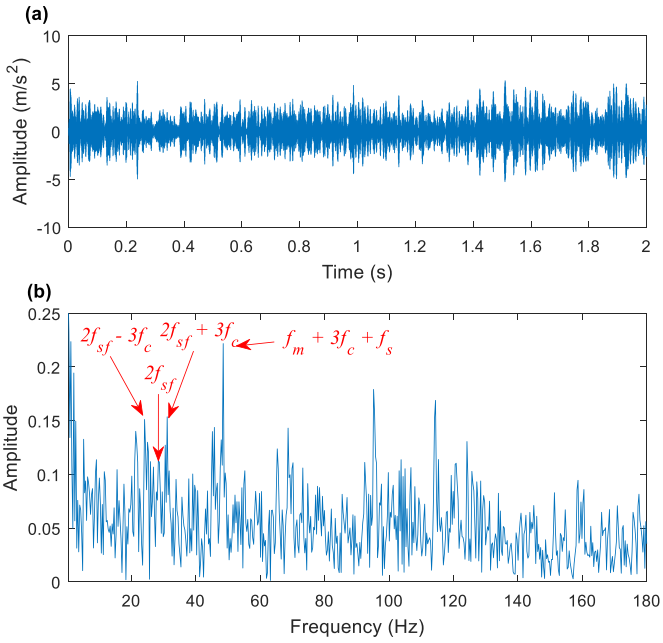

Figure 9. RSVD-ESA results: (a) waveform of RSVD processed signal, (b) envelope spectrum.

In addition, the vibration signal is also processed by the FK method, and the results are depicted in figure 10. As shown in figure 10(a), the most sensitive central frequency and bandwidth of the FK filtering are 1041.7 Hz and 416.7 Hz, respectively. Figure 10(b) illustrates the time domain waveform of the FK filtered signal, it not only can be seen from figure that there is no obvious periodic characteristic, but indicates that there are interferences of high amplitude of random noise and

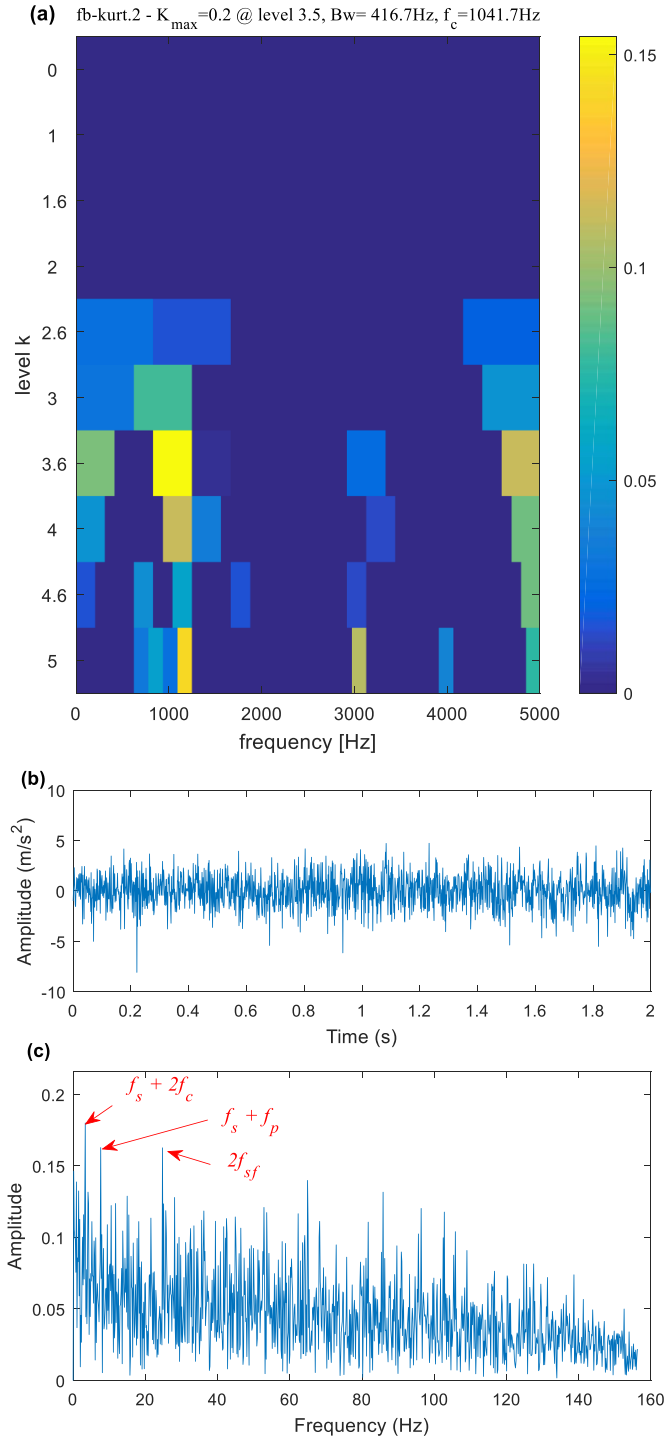

Figure 10. FK results: (a) kurtogram, (b) waveform of processed signal, (c) envelope spectrum.

pulses in the signal. Figure 10(c) illustrates the envelope spectrum of the FK filtered signal, from which the fault feature of the second harmonic frequency of sun gear fault can be identified. However, its amplitude has little difference from the surrounding noise or interferences, which affects the accuracy of feature extraction.

The fault features extracted by the proposed ISVD-ESA method is more clearly than the other two. The comparison results of figures 8 and 9 indicate that the proposed ISVD-ESA

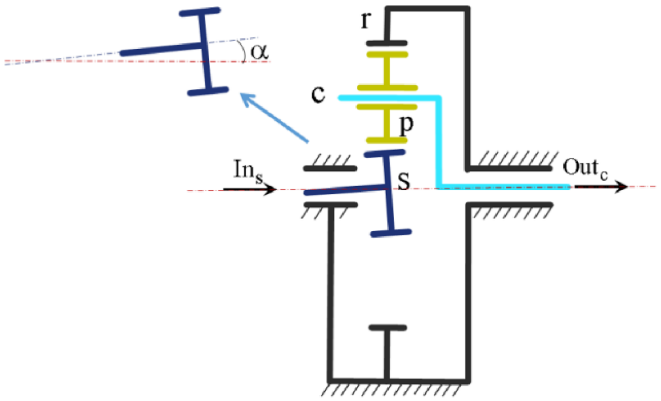

Figure 11. Schematic diagrams of the misalignment planetary gearbox.

method is better than that of the RSVD-ESA method in the performance of complex coupled feature enhancement. The result of FK filter is disturbed by more interferences and noise than the former two. Therefore, the filtered signal of FK is still a mixture of multi-path and multi-source signal. To sum up, the proposed ISVD-ESA method can be used to detect the tooth pitting fault of sun gear for the planetary gearbox.

4.3. Fault detection of sun gear misalignment

Misalignment is a common phenomenon in the cases of loose installation or long-term operation of rotating machinery. It is more difficult to detect the misalignment than the failure in the form of damage for the planetary gearbox, because the sun gear is designed to float in the radial direction and the impulse energy generated by misalignment is weaker than that of interferences until the planetary gearbox is damaged. However, it is the main reason for the damage of rotating machineries in engineering. Therefore, an experimental test of sun gear angular misalignment is designed in this case, which is made by wedging a 1.0 mm gasket into the base of the planetary gearbox on the test bed. The schematic diagram of this experiment is illustrated in figure 11, from which the gap between sun gear and planetary gears is utilized to represent the angular misalignment between the sun gear and the central axis of the planetary gearbox. The vibration signal of the planetary gearbox is collected under the condition of 30% rated speed and 50% rated load, and the sun gear shaft speed is 439 rpm. The characteristic frequencies are listed in table 4.

Figure 12(a) presents the time domain waveform of the vibration signal, from which the oscillation phenomenon of the vibration signal can be seen. Figure 12(b) illustrates the amplitude spectrum of the measured signal, in which all the characteristic frequencies are submerged by interferences and noise. Figure 12(c) illustrates the envelope spectrum of the measured signal, in which the features of $f_m - f_s - f_p - 3f_c$, $f_m - f_s$ and $2(f_m - f_s - f_p - 3f_c)$ can be identified, these features show that the vibration signal is modulated by sun gear, planetary gears and planetary carrier in the transmission process, and are incapable of characterizing the misalignment of the sun gear.

Table 4. Characteristic component frequencies of the diagnosed planetary gearbox.

Characteristic Frequency	Relationship to input frequency	Value (Hz)
Sun gear shaft (f_{as})	f_{as}	7.31
Sun gear (f_s)	$f_{as} \cdot z_r/(z_s + z_r)$	6.30
Sun gear fault (f_{sf})	$N_p \cdot f_{as} \cdot z_r/(z_s + z_r)$	18.89
Planetary gear (f_p)	$f_{as} \cdot z_s \cdot z_r/[z_p \cdot (z_s + z_r)]$	2.42
Planetary gear fault (f_{pf})	$2f_{as} \cdot z_s \cdot z_r/[z_p \cdot (z_s + z_r)]$	4.84
Planetary carrier (f_c)	$f_{as} \cdot z_s/(z_s + z_r)$	1.02
Internal ring gear fault (f_{rf})	$N_p \cdot f_{as} \cdot z_s/(z_s + z_r)$	3.05
Meshing (f_m)	$f_{as} \cdot z_s \cdot z_r/(z_s + z_r)$	62.96

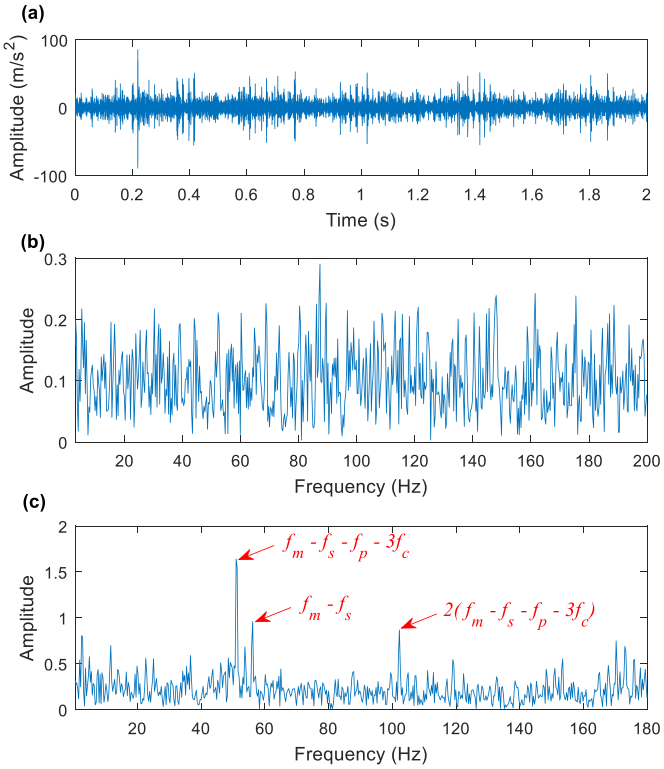

Figure 12. Experimental signal: (a) waveform, (b) amplitude spectrum, (c) envelope spectrum.

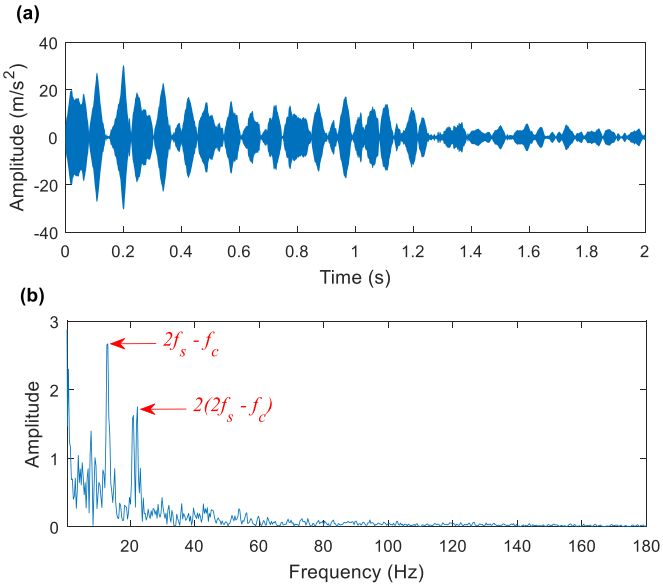

Figure 13. ISVD-ESA results: (a) waveform of ISVD processed signal, (b) envelope spectrum.

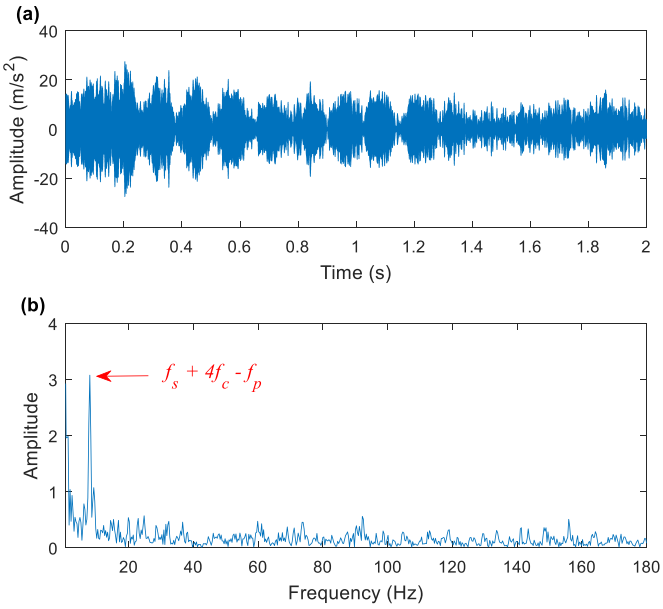

Figure 14. RSVD-ESA results: (a) waveform of RSVD processed signal, (b) envelope spectrum.

The proposed ISVD-ESA method is applied to process the measured vibration signal, and the results are shown in figure 13. The matrixing parameters k is set to $k = 6115$ according to step 1 of ISVD-ESA strategy. The time domain waveform of the output signal of ISVD is shown in figure 13(a). It can be seen that the amplitude of the signal decreases with time. This phenomenon shows that the attenuation effect of the vibration response of the vibration source increases with time, which may be because the modulation source is rotating away from the vibration sensor, and with the rotation of the planet carrier, the transmission path becomes longer with time. Figure 13(b) illustrates the result of the ISVD-ESA method, in which the characteristic frequencies of $2f_s + f_c$ and $2(2f_s - f_c)$ are clearly detected. In rotating machinery, misalignment can be diagnosed by the energies of harmonic frequency of a rotating part larger than its rotating frequency. The f_c is an interference frequency modulated into the signal during signal transmission. Therefore, the presence of energetic frequencies of $2f_s$ and $4f_s$ can testify that the sun gear is misalignment.

The RSVD-ESA method is also utilized to analyze the same signal, the processing steps are similar with the ISVD-ESA method in figure 13. Figure 14(a) shows the time domain waveform of the output signal of RSVD. The amplitude of the signal also slowly decreases over time in figure 14(a). The result of RSVD-ESA is depicted in figure 14(b). It can be seen that the frequency of $f_s + 4f_c - f_p$ can be clearly identified. The transmission path from the sun gear to the sun gear shaft, from

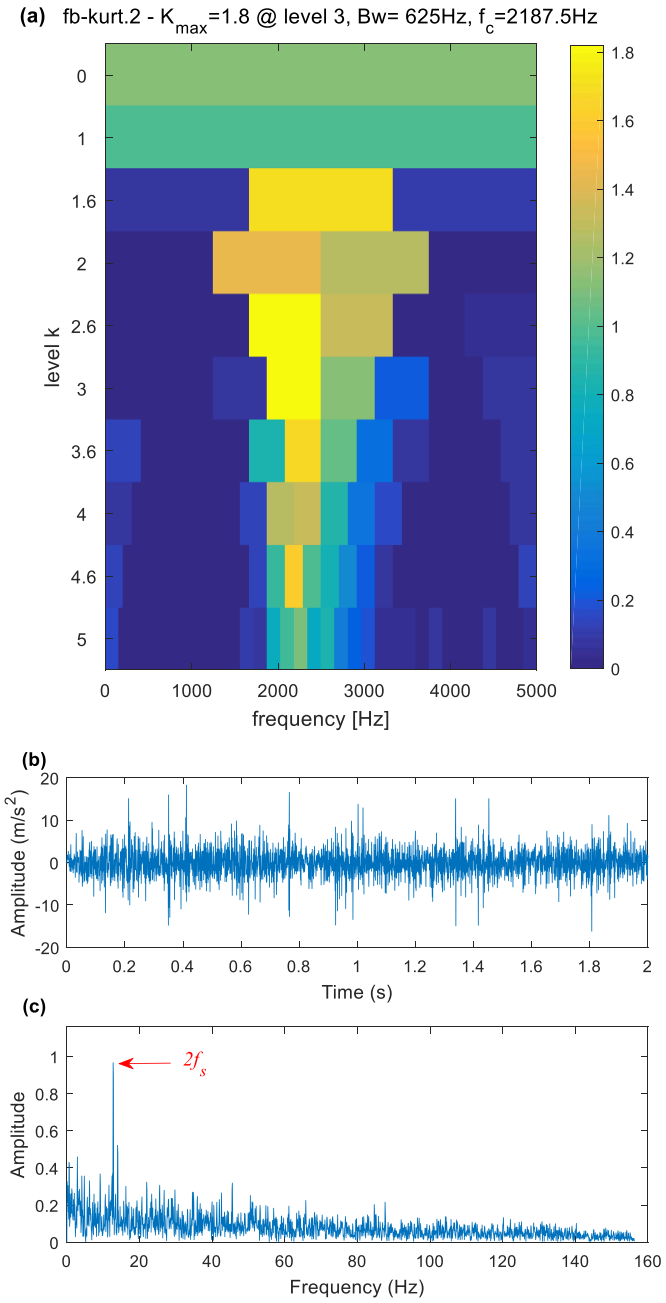

Figure 15. FK results: (a) kurtogram, (b) waveform of FK processed signal, (c) envelope spectrum.

the shaft to the bearing seat, and from the bearing seat to the vibration sensor on the ring gear is one of the main transmission paths of the vibration signal of the planetary gearbox. The frequency extracted by RSVD-ESA may be modulated by the vibration signal transmission. Therefore, the sun gear misalignment cannot be extracted by the RSVD-ESA method.

The same measured data is also processed by the FK method, and the results are depicted in figure 15. Figure 5(a) shows the time domain waveform of the FK filtered signal, from which the most sensitive central frequency and bandwidth of the FK filtering are 2187.5 Hz and 625 Hz, respectively. Figure 15(b) illustrates the time domain waveform of the FK filtered signal, from which can be seen several high amplitude random pulses. Figure 15(c) illustrates the envelope spectrum of the FK filtered signal. It can be seen, the amplitude of envelope spectrum is mixed with a variety of noise and interferences, and the characteristic frequency of $2f_s$ is clearly extracted. However, this frequency may be modulated by the vibration signal transmission, and cannot reveal the existence of the sun gear misalignment. Therefore, the sun gear misalignment cannot be extracted by the FK method.

The comparison of ISVD-ESA, RSVD-ESA and FK in the sun gear misalignment detection and fault features enhancement of planetary gearbox shows that only the ISVD-ESA method successfully extracted the fault features. In the comparison of figures 13(a) and 14(a), it can be found that the proposed ISVD method is better than that of the RSVD method in the performance of denoising. To sum up, the performance of the proposed ISVD-ESA method is superior compared to the methods of RSVD-ESA and FK in sun gear misalignment of the planetary gearbox.

5. Conclusion

In order to overcome the difficulty in extracting fault features from the vibration signal of planetary gearbox, an ISVD-ESA method is proposed in this paper. The ISVD-ESA makes full use of the advantage of blind source separation of SVD method, and the ability of negentropy and CA in non-Gaussian characteristics recognition. The modulated fault characteristics in different SVCSs are correlated. However, the output signal of ISVD method is composed of different SVCSs which are independent with each other. Therefore, the ESA is applied to detect the fault features. The effectiveness and feasibility of the ISVD-ESA for the fault diagnosis of a planetary gearbox are demonstrated through experimental cases of sun gear tooth pitting and sun gear misalignment. The results illustrate that the proposed ISVD-ESA method is superior to the RSVD-ESA and FK in detection of sun gear faults of planetary gearbox.

Data availability statement

The data generated and/or analyzed during the current study are not publicly available for legal/ethical reasons but are available from the corresponding author on reasonable request.

Acknowledgments

The work was supported by the National Natural Science Foundation of China (NSFC) under Grant No. 51875166 and the foundation project of the key Laboratory of Science and Technology on Integrated Logistics Support, National University of Defense Technology under Grant No. 6142003200102.

ORCID iDs

Zhaoyang Shen https://orcid.org/0000-0002-9872-9363

Dong Zhen https://orcid.org/0000-0002-5047-3346
Fengshou Gu https://orcid.org/0000-0003-4907-525X

References

[1] Liang X, Zuo M J and Feng Z 2018 Dynamic modeling of gearbox faults: a review *Mech. Syst. Signal Process.* **98** 852–76
[2] Wang T, Han Q, Chu F and Feng Z 2019 Vibration based condition monitoring and fault diagnosis of wind turbine planetary gearbox: a review *Mech. Syst. Signal Process.* **126** 662–85
[3] Li Y, Li G, Yang Y, Liang X and Xu M 2018 A fault diagnosis scheme for planetary gearboxes using adaptive multi-scale morphology filter and modified hierarchical permutation entropy *Mech. Syst. Signal Process.* **105** 319–37
[4] Cheng Z, Gao M, Liang X and Liu L 2020 Incipient fault detection for the planetary gearbox in rotorcraft based on a statistical metric of the analog tachometer signal *Measurement* **15** 107069
[5] Feng Z, Lin X and Zuo M J 2016 Joint amplitude and frequency demodulation analysis based on intrinsic time-scale decomposition for planetary gearbox fault diagnosis *Mech. Syst. Signal Process.* **72–73** 223–40
[6] Liu J, Tang C and Pan G 2021 Dynamic modeling and simulation of a flexible-rotor ball bearing system *J. Vib. Control* 1–15
[7] Li J and Xu Z 2022 A simulation investigation of lubricating characteristics for a cylindrical roller bearing of a high-power gearbox *Tribol. Int.* **167** 107373
[8] Wang D, Peng Z and Xi L 2020 The sum of weighted normalized square envelope: a unified framework for kurtosis, negative entropy, Gini index and smoothness index for machine health monitoring *Mech. Syst. Signal Process.* **140** 106725
[9] Hu Y, Tu X and Li F 2019 High-order synchrosqueezing wavelet transform and application to planetary gearbox fault diagnosis *Mech. Syst. Signal Process.* **131** 126–51
[10] Wan S T and Peng B 2019 The FERgram: a rolling bearing compound fault diagnosis based on maximal overlap discrete wavelet packet transform and fault energy ratio *J. Mech. Sci. Technol.* **33** 157–72
[11] Qin Y, Xing J and Mao Y 2016 Weak transient fault feature extraction based on an optimized Morlet wavelet and kurtosis *Meas. Sci. Technol.* **27** 085003
[12] Ren H, Liu W, Shan M and Wang X 2019 A new wind turbine health condition monitoring method based on VMD-MPE and feature-based transfer learning *Measurement* **148** 106906
[13] Li J, Wang H, Zhang J, Yao X and Zhan Y 2019 Impact fault detection of gearbox based on variational mode decomposition and coupled underdamped stochastic resonance *ISA Trans.* **95** 320–9
[14] Li Y, Li G, Wei Y, Liu B and Liang X 2018 Health condition identification of planetary gearboxes based on variational mode decomposition and generalized composite multi-scale symbolic dynamic entropy *ISA Trans.* **81** 329–41
[15] Pan H, Zheng J, Yang Y and Cheng J 2021 Nonlinear sparse mode decomposition and its application in planetary gearbox fault diagnosis *Mech. Mach. Theory* **155** 104082
[16] Miao Y, Zhao M, Yi Y and Lin J 2020 Application of sparsity-oriented VMD for gearbox fault diagnosis based on built-in encoder information *ISA Trans.* **99** 496–504
[17] Guo J, Zhen D, Li H, Shi Z, Gu F and Ball A D 2020 Fault detection for planetary gearbox based on an enhanced average filter and modulation signal bispectrum analysis *ISA Trans.* **101** 408–20
[18] Xu L, Chatterton S and Pennacchi P 2021 Rolling element bearing diagnosis based on singular value decomposition and composite squared envelope spectrum *Mech. Syst. Signal Process.* **148** 107174
[19] Zhao X and Ye B 2010 Difference spectrum theory of singular value and its application to the fault diagnosis of headstock of lathe *J. Mech. Eng.* **46** 100–8
[20] Xu X, Zhao M and Lin J 2017 Detecting weak position fluctuations from encoder signal using singular spectrum analysis *ISA Trans.* **71** 440–7
[21] Mao Y, Jia M and Yan X 2020 A new bearing weak fault diagnosis method based on improved singular spectrum decomposition and frequency-weighted energy slice bispectrum *Measurement* **166** 108235
[22] Guo M, Li W, Yang Q, Zhao X and Tang Y 2020 Amplitude filtering characteristics of singular value decomposition and its application to fault diagnosis of rotating machinery *Measurement* **154** 107444
[23] Miao Y, Zhao M and Lin J 2019 Periodicity-impulsiveness spectrum based on singular value negentropy and its application for identification of optimal frequency band *IEEE Trans. Ind. Electron.* **66** 3127–38
[24] Logan A, Cava D G and Liśkiewicz G 2021 Singular spectrum analysis as a tool for early detection of centrifugal compressor flow instability *Measurement* **173** 108536
[25] Zhao X and Ye B 2011 Selection of effective singular values using difference spectrum and its application to fault diagnosis of headstock *Mech. Syst. Signal Process.* **25** 1617–31
[26] Li H, Liu T, Wu X and Chen Q 2019 Research on bearing fault feature extraction based on singular value decomposition and optimized frequency band entropy *Mech. Syst. Signal Process.* **118** 477–502
[27] Zhao M and Jia X 2017 A novel strategy for signal denoising using reweighted SVD and its applications to weak fault feature enhancement of rotating machinery *Mech. Syst. Signal Process.* **94** 129–47
[28] Lyu X, Hu Z, Zhou H and Wang Q 2019 Application of improved MCKD method based on QGA in planetary gear compound fault diagnosis *Measurement* **139** 236–48
[29] Minhas A S, Kankar P K, Kumar N and Singh S 2021 Bearing fault detection and recognition methodology based on weighted multiscale entropy approach *Mech. Syst. Signal Process.* **147** 107073
[30] Tănăsescu A and Popescu P G 2019 A fast singular value decomposition algorithm of general k-tridiagonal matrices *J. Comput. Sci.* **31** 1–5
[31] Wang C, Li H, Ou J, Hu R, Hu S and Liu A 2020 Identification of planetary gearbox weak compound fault based on parallel dual-parameter optimized resonance sparse decomposition and improved MOMEDA *Measurement* **165** 108079
[32] Shen Z, Shi Z, Zhen D, Zhang H and Gu F 2020 Fault diagnosis of planetary gearbox based on adaptive order bispectrum slice and fault characteristics energy ratio analysis *Sensors* **20** 2433
[33] Guo J, Zhang H, Zhen D, Shi Z, Gu F and Ball A D 2020 An enhanced modulation signal bispectrum analysis for bearing fault detection based on non-Gaussian noise suppression *Measurement* **151** 107240
[34] Miao Y, Zhang B, Yi Y and Lin J 2021 Application of improved reweighted singular value decomposition for gearbox fault diagnosis based on built-in encoder information *Measurement* **168** 108295
[35] Chen Y, Liang X and Zuo M J 2020 An improved singular value decomposition-based method for gear tooth crack

detection and severity assessment *J. Sound Vib.* **468** 115068
[36] Shirokov D S 2021 A note on the hyperbolic singular value decomposition without hyperexchange matrices *J. Comput. Appl. Math.* **391** 113450
[37] Wang D, Zhong J, Li C and Peng Z 2021 Box-Cox sparse measures: a new family of sparse measures constructed from kurtosis and negative entropy *Mech. Syst. Signal Process.* **160** 107930
[38] Li G, Tang G, Luo G and Wang H 2019 Underdetermined blind separation of bearing faults in hyperplane space with variational mode decomposition *Mech. Syst. Signal Process.* **120** 83–97
[39] Tang S, Yang J and Ai D 2018 *Theory of Weak Signal Processing* 4th edn (Beijing: Beijing University of Technology Press)
[40] McDonalda G L, Zhao Q and Zuo M J 2012 Maximum correlated Kurtosis deconvolution and application on gear tooth chip fault detection *Mech. Syst. Signal Process.* **33** 237–55
[41] Wang L, Liu Z, Cao H and Zhang X 2020 Subband averaging kurtogram with dual-tree complex wavelet packet transform for rotating machinery fault diagnosis *Mech. Syst. Signal Process.* **142** 106755
[42] He G, Ding K, Wu X and Yang X 2019 Dynamics modeling and vibration modulation signal analysis of wind turbine planetary gearbox with a floating sun gear *Renew. Energy* **139** 718–29
[43] Liu Z, Lei Y, Liu H, Yang X and Song W 2020 A phenomenological model for investigating unequal planet load sharing in epicyclic gearboxes *Mech. Syst. Signal Process.* **135** 106414